Force-Reversible and Energetic Indole-Mg-Indole Interaction for Designing Toughened and Multifunctional High-Performance Thermosets

Li Yang, Yicheng Li, Mengqi Du, Yiting He, Yang Lan, Qiang Yin, Fanghua Zhu and Guanjun Chang**

Prof. L. Yang, Dr. Y. C, Li, Dr. M. Q. Du, Prof. G. J. Chang
State Key Laboratory for Environment-Friendly Energy Materials & School of Material Science and Engineering, Southwest University of Science and Technology, Mianyang, 621010, P. R. China
E-mail: gjchang@mail.ustc.edu.cn
Y. He, Dr. Y. Lan
Centre for Nature-Inspired Engineering, Department of Chemical Engineering, University College London, London, WC1E 7JE, United Kingdom
E-mail: yang.lan@ucl.ac.uk
Prof. Q. Yin, Dr. F. H. Zhu
Research Center of Laser Fusion, China Academy of Engineering Physics, Mianyang, 621900, P. R. China

Keywords: high-performance thermoset, functional polymer, force-reversible interaction

Abstract: Non-covalent crosslinking has provided versatile and affordable solutions for the design of tough soft polymer materials, but it was not applied in stiff high-performance thermosets. Here we report a supramolecular approach for the design of tough high-performance thermosets by using the noncovalent sandwich-structural indole-Mg-indole complexes acting as the force-reversible and energetic crosslinking points, evading the inherent trade-off between mechanical strength and ductility for high-performance thermosets. Compared to traditional epoxy polymer materials, the indole-Mg-indole crosslinks of the network enables synchronously enhancement of mechanical strength and ductility owing to the increased interaction-energy and efficient dissociation and reassociation behaviors given by the dynamic indole-Mg-indole complexes, which is quite challenging to achieve by conventional chemical methods. In addition, local manipulation of crosslinking confers the resulting thermosets with multiple fast stimuli-responsive functions, such as recyclability; healability and adhesion.

1. Introduction

Tensile strength and ductility are two important properties for polymeric materials, which dictates their applications in areas such as aerospace, machinery and electronics field. Generally, tensile strength of polymeric materials can be enhanced by covalent crosslinking, leading to widely used thermoset materials. However, increasing tensile strength of polymeric materials in this manner often leads to a decrease in their ductility.[1] For example, the tensile strengh of epoxy resin, a typical thermoset material, can be generally enhanced after curing (covalently crosslinking). Yet, epoxy resin also becomes brittle and hard to be melted for reshaping after curing.[2,3] The trade-off between tensile strength and ductility of thermosets has hampered their applications and recyclability. Recently, the employment of non-covalent crosslinking via hydrogen bonding, electrostatic, and metal-ligand interactions to replace covalent crosslinking in polymeric materials shows a significant effect on improving their ductility while maintaining the tensile strength. This is because externally applied energy can effectively be dissipated upon the association and dissociation of the supramolecular interactions within the polymeric materials.[4] This supramolecular approach can be easily applied to soft polymeric materials such as hydrogels, in which polymer chains are not totally arrested as solvents exist. However, it is barely explored in tuning the tensile strength and ductility of stiff thermosets.[5]

This paper reports a supramolecular approach for high-performance thermosets by using dynamic indole-Mg^{2+}-indole interaction, which is a sandwich-like, strong, and noncovalent interaction between Mg^{2+} and the π-face of indole (**Figure 1**A, 1B, 1C). Calculation results indicate that Mg cation is positioned above the benzyl ring of the indole ring. HOMO π-electron density is delocalized towards the Mg ion, creating a partial electron deficiency on the indole ring. The $(Ot\text{-}Bu)^-$ anion forms hydrogen bonds to the indole amine, creating a compensatory, stabilizing partial negative charge on the indole (Figure 1C). The interaction energy of indole-Mg^{2+}-indole complex is comparable with traditional covalent bonds (311 kJ/mol versus ~350 kJ/mol).[6] Moreover, maximal constraining force of indole-Mg^{2+}-indole bond in $Mg(Ot\text{-}Bu)^2$-

Indole complex is weaker than a traditional C-C or C-N bond (2.4 nN versus ~6.0 nN) and higher than that of traditional non-covalent bonds (Figure 1D, 1E).[7] It indicates that, in the stiff thermoset, the indole-Mg-indole bond can break preferentially, resulting in efficient energy dissipation of an external mechanical stress. In addition, the range of indole-Mg-indole interaction is relatively wide in cation-π distances,[8] endowing indole-Mg-indole complex with efficient association and dissociation when subjected to an external force (Figure 1D, 1E). It is concluded that the association and dissociation of the indole-Mg-indole bond could occur simultaneously at ambient temperature in dry-state, enabling the thermosets with unprecedentedly enhancement in both mechanical strength and ductility via simultaneous conformational adjustment of polymer segment to maintain the network integrity.

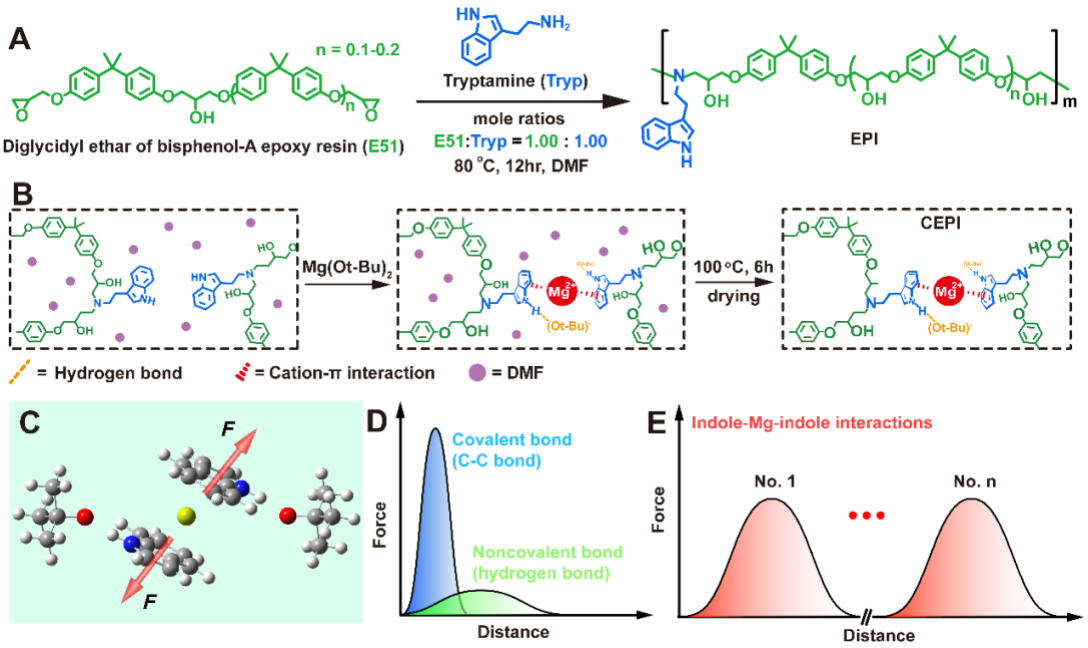

Figure 1. Synthesis, crosslinking manipulation, and noncovalent interaction of stiff thermosets. (A) Synthetic pathway of linear EPI. (B) A scheme of the indole-Mg-indole complex formation. (C) Theoretically calculated the restored forces and free energies of dissociation of indole-Mg-indole. The calculated restored forces and interaction distance for traditional chemical bond, traditional noncovalent bond (D) and indole-Mg-indole (E), and the No. n is the dissociation and rebuild times of one indole-Mg-indole bond before the polymer film was destroyed when subjected to an external force.

2. Results and Discussion

2.1. Preparation of High-Performance Thermosets

To demonstrate the concept, a linear polymer EPI is first synthesized via copolymerization of diglycidyl ether of bisphenol-A epoxy resin (E51) and Tryptamine (Tryp) at the molar ratio of 1:1 (Figure 1A). Subsequent treatment with magnesium di-tert-butoxide ($Mg(Ot\text{-}Bu)_2$) forms supramolecularly crosslinked high-performance thermosets (Figure 1B). The crosslinking density of the thermosets is readily controlled through the monomer feed ratios of Mg^{2+} to indole. The resulting thermosets are denoted as CEPI-x, where x represents the molar fraction of Mg^{2+} in the feed. The corresponding thermoset films are prepared by solvent casting method. The experimental procedures and characterization are described in detail in the *Experimental Section* and *Supporting Information*. Here, we chose the CEPI-10 as a typical example to present our results. At ambient temperature, the CEPI-10 film is semitransparent, non-adhesive and insoluble solids (Figure S3, Table S1).

2.2. Verification of indole-Mg-indole interaction in CEPI Network

We performed a series of experiments and simulations to study the molecular mechanism of these microscopic changes in response to alternative external force treatments. **Figure 2**A shows the absorption spectra of the polymers in the presence and absence of Mg^{2+}, together with the difference spectra of CEPI-10 minus EPI. The spectrum clearly reveals a pair of negative/positive intensity changes generated at 233/272 nm, confirming stable cation-π interactions between Mg^{2+} and the indole rings.[9] The *in-situ* stress relaxation-UV-vis spectra are carried out for CEPI-10 film at ~100 °C (higher than its glass transition temperature) (Figure 2B, 2C). The results clearly show a blue shift of π-π* absorption peak of indole groups, indicating the indole-Mg-indole bond could form gradually in the network during stress relaxation. In addition, the linear EPI film exhibits a strong fluorescence (λ_{exc} = 365 nm). After Mg^{2+} curing, the fluorescence intensity of the CEPI-10 film decrease significantly due to the conjugate structure changing before and after crosslinking (Figure 2D).[10] Based on this, the in-situ stress relaxation-RF spectrum is used for tracking fluorescence intensity changes for CEPI-10 film in the process of stress relaxation. As expected, the results show that the

fluorescence intensity decreases gradually during stress relaxation (Figure 2E), indicating the dynamic association and dissociation of the indole-Mg-indole bond under an external force.

According to the calculations, in the dissociation of indole-Mg(Ot-Bu)$_2$ complexes pulled at the indole-Mg-indole linkages, such changes occur at a maximum restored force of 2.4 nN, which is a comparable value to that of previously reported force-activated covalent bonds (Figure 2F),[7,11] indicating that the indole-Mg-indole interaction could break preferentially compared to traditional chemical bonds. The dissociation of indole-Mg-indole interaction also exhibit high energy dissipation (301 kJ/mol) due to this long rang interactions (ΔL = 5.6 Å) (Figure 2F). Taken together, the indole-Mg-indole complexes acting as the energetic crosslinking points plays an important role in designing for high-performance toughing thermosets due to its unique mechanical behaviors.

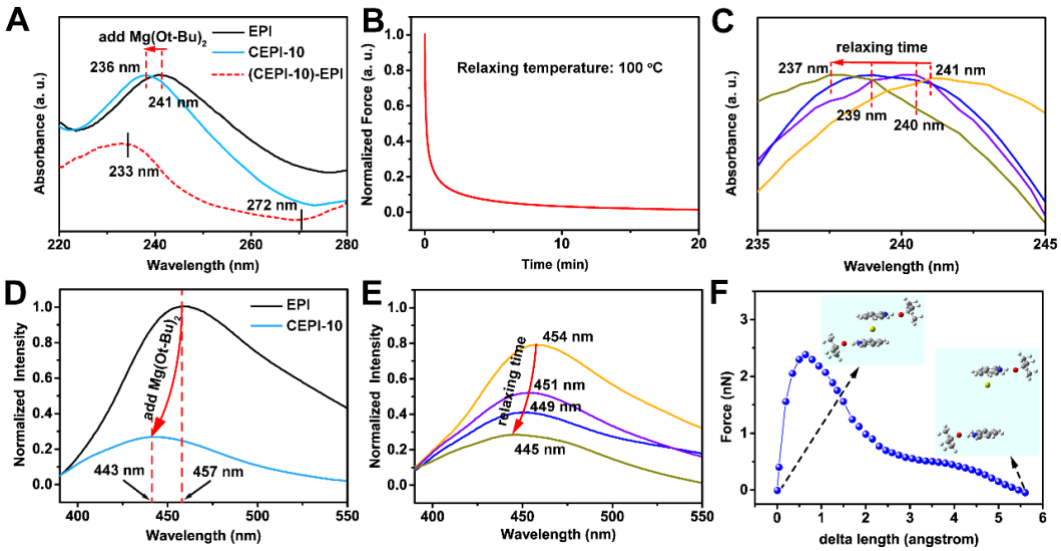

Figure 2. Mechanics experiments of force-activated reversible behaviors of the indole-Mg-indole in dry-state polymer film. (A) UV-vis spectra of EPI (black line), CEPI-10 (blue line) and the difference spectrum of CEPI-10 minus CPI. (B) Stress relaxation curve of CEPI-10 at 100°C. (C) The *in-situ* stress relaxation-UV-vis spectra. (D) Fluorescence spectra of EPI (black line) and CEPI-10 (blue line). (E) The *in-situ* stress relaxation-RF spectra of CEPI-10. (F) Theoretically calculated the restored force of indole-Mg-indole complexes dissociation as a function of indole-Mg-indole bonding length at 1 atm, 298.15 K.

2.3. Mechanical Properties

Uniaxial tensile tests show a pronounced increase in both tensile strength and toughness of the thermo-stable CEPI-10 film compared with the EPI film and other CEPI-n (n = 5, 15, 20) films

(**Figure 3**A, Figure S4 and S5), Figure 3A shows that both tensile strength and toughness of the polymer films increase when crosslinking density increases to 10%, yet decreases from 10% to 15%. The changes are similar to that of soft vulcanized rubber.[12] When the crosslinking density is further increased from 15% to 20%, the ductility of the polymer film decreases rapidly while the tensile strength barely increased, resulting in brittle fracture of the polymer film. The dynamic net effect shows a ~2-fold increase in tensile strength, from σEPI = 62 to σCEPI-10 = 108 MPa; and a corresponding 4-fold increase in elongation at break, from 5.4% to 21.1% (Figure 3A). Accordingly, there is a 11-fold increase in tensile toughness (energy density), from 1.9 to 21.1 MJ/cm^3 (Figure 3B). Compared to traditional epoxy polymer materials, the indole-Mg-indole crosslinks within our thermoset enables the enhancement of both mechanical strength and ductility owing to the increased interaction-energy and efficient dissociation and reassociation behaviors given by the dynamic indole-Mg-indole complexes, which is quite challenging to achieve by conventional covalent crosslinking methods (Figure S6A).

Considering the CEPI-10 film exhibits the excellent mechanical behaviors, here we propose a strengthening and toughening mechanism. Upon cyclic loading of Mg(Ot-Bu)$_2$-Indole complex crosslinked CEPI-10 film (Figure 3C), energy dissipation is manifested as prominent hysteresis loops for strains beyond the linear regime. At small applied strains (ε < 5 %, Figure 3C,D) after a loading-unloading cycle, the unbroken reversible indole-Mg-indole bond act as a conventional chemically cross-linkage, entropically drive the network back to the unstretched state after the force is released, the mechanical behavior conforms to Hooke's law.[13] At medium applied strains (ε, ~ 10 %, Figure 3C,D), the indole-Mg-indole bond in the network begin to break, entropically drive the network almost back to the unstretched state when increasing the temperature (~ T_g 90 °C) to remove forced high-elastic deformation. At larger applied strains (ε > 15 %), the breakage of reversible indole-Mg-indole bonds occurs during elongation while their reformation can happen at newly accessible sites. The network is in this case permanently deformed (non-recoverable) from the standpoint of thermodynamics,

and the residual strain would be observed even at temperature exceeding its glass transition temperature (~ 90 ºC) (Figure 3C,D).

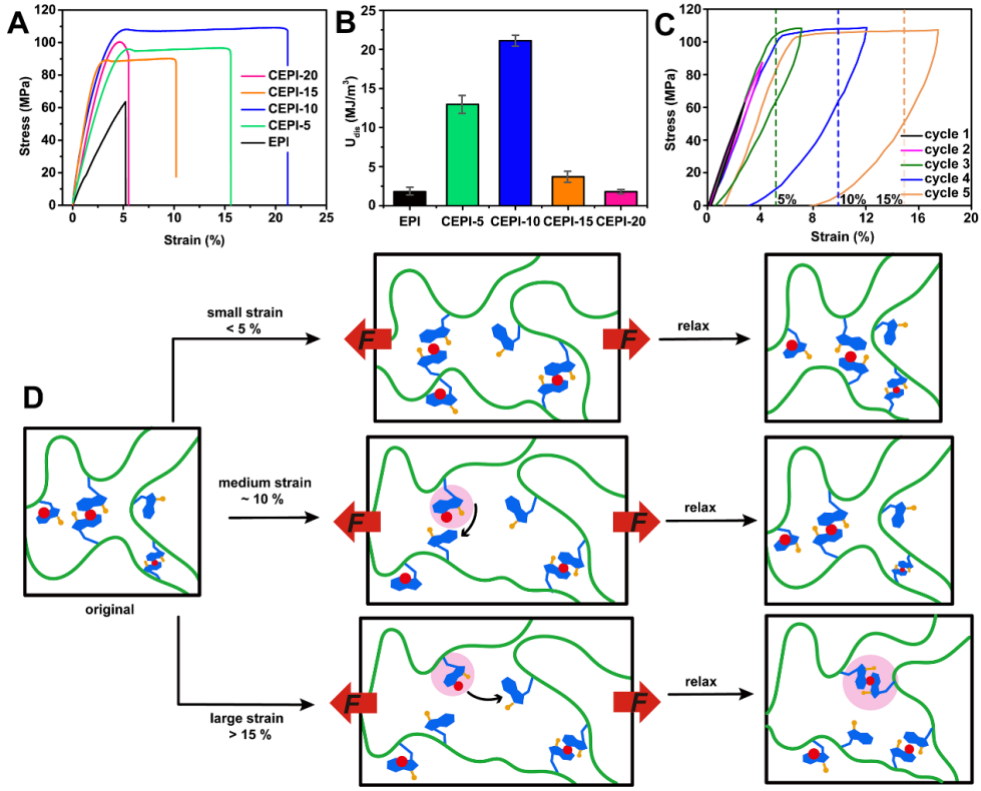

Figure 3. Mechanical behaviors. (A) Stress-strain curves of different polymer films. (B) Energy dissipations when applying an external force on the films. (C) Cyclic stretching of the CEPI-10 film. (D) Proposed mechanism for the strain recovery.

The divalent metal compound is an essential component to form the sandwich-structural crosslinks. We studied the influence of different divalent metal cations on the mechanical properties of the crosslinked films with the same crosslinking density, and all the crosslinked polymer films exhibited excellent and similar mechanical properties (Figure S6B). Considering the solubility of salts in organic solvents and the costs of the divalent metal compounds, we chose the $Mg(Ot\text{-}Bu)_2$ as a typical example to prove the concept.

2.4. Recycling Behaviors

The reversible installation and removal of the indole-Mg-indole bond in $Mg(Ot\text{-}Bu)_2$-Indole complex enables broken CEPI-10 sample to be recycled by a three-step procedure (**Figure 4**A). (i) The crosslinked CEPI-10 sample is gradually dissolved in NMP solvent upon the addition

of pyrophosphate (PPi) (0.3 M in DMF) due to stronger coordination ability between PPi and Mg ions (I, II, and III in Figure 4A).[14] (ii) The mixture is poured into cold water, and the precipitates are filtered and then dried at 100 °C under vacuum to convert back to the original linear EPI again (IV and V in Figure 4A). (iii) The crosslinked CEPI-10 sample could regain by adding $Mg(Ot\text{-}Bu)_2$ (VI in Figure 4A). The supramolecular crosslinking within the thermosets allows another possible approach to recycle the thermoset. The crosslinked CEPI-10 thermoset could also be recycled mechanically via melting and reforming (Figure 4D). (i) Original CEPI-10 sample is crushed into parts (I and II in Figure 4D). (ii) Compression molding of the melted debris enables the "2nd generation" CEPI-10 sample (III and IV in Figure 4D). The recycled samples have been subjected to multiple recycling treatments and still have nearly the same stress-strain behavior as the original sample (Figure 4B, 4C).

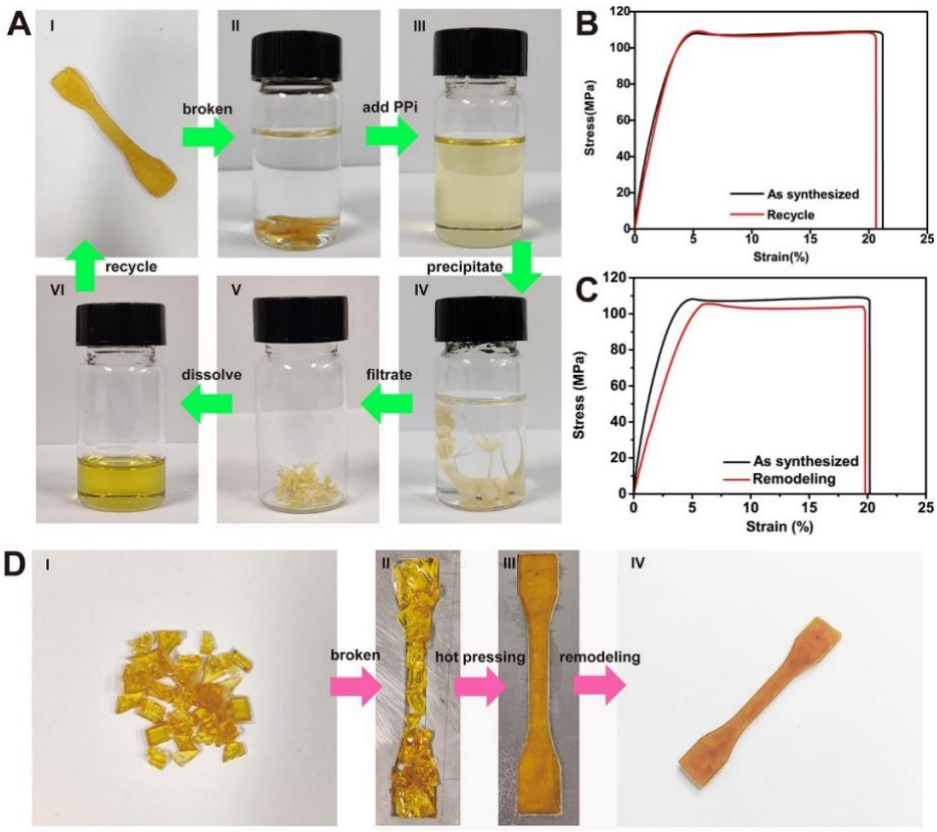

Figure 4. Recycling. (A) CEPI-10 sample (I), broken CEPI-10 cannot dissolve in NMP even at high temperature (II), broken CEPI-10 can dissolve in NMP in the presence of PPi (III), precipitate in water (IV), filter and dry (V), linear EPI dissolved in NMP (VI). (B) Stress-strain curves of original and recycled CEPI-10 films. (C) Stress-strain curves of original and remodeling CEPI-10 films. (D) Remodeling process of the broken CEPI-10 sample.

2.5. Healing and Adhesion

Inspired by the skin healing,[15] we realized that cracks of CEPIs polymer materials are potentially healable with help of Mg-ion solution. To test the feasibility, a CEPI-10 film is damaged to create a well-defined cut with thickness of approximately ~ 5 μm using a razor blade (I in **Figure 5**A). Mg-ion solution is introduced to the surface of the crack. The CEPI-10 film, which contacts the Mg-ion solution, is dissolved and the surface of the cut is healed upon solvent evaporation (III in Figure 5A). AFM shows the topology of the damaged area before and after healing, and it is found that the depth profile of the cut area is identical to other untouched region after the healing (II, IV in Figure 5A). In addition, the healing property of a torn CEPI-10 sample is performed, and the torn sample exhibit a similar healing effect (V and VI in Figure 5A). Two types of healing samples both have nearly the same stress-strain behaviors with the original CEPI-10 sample (Figure 5B).

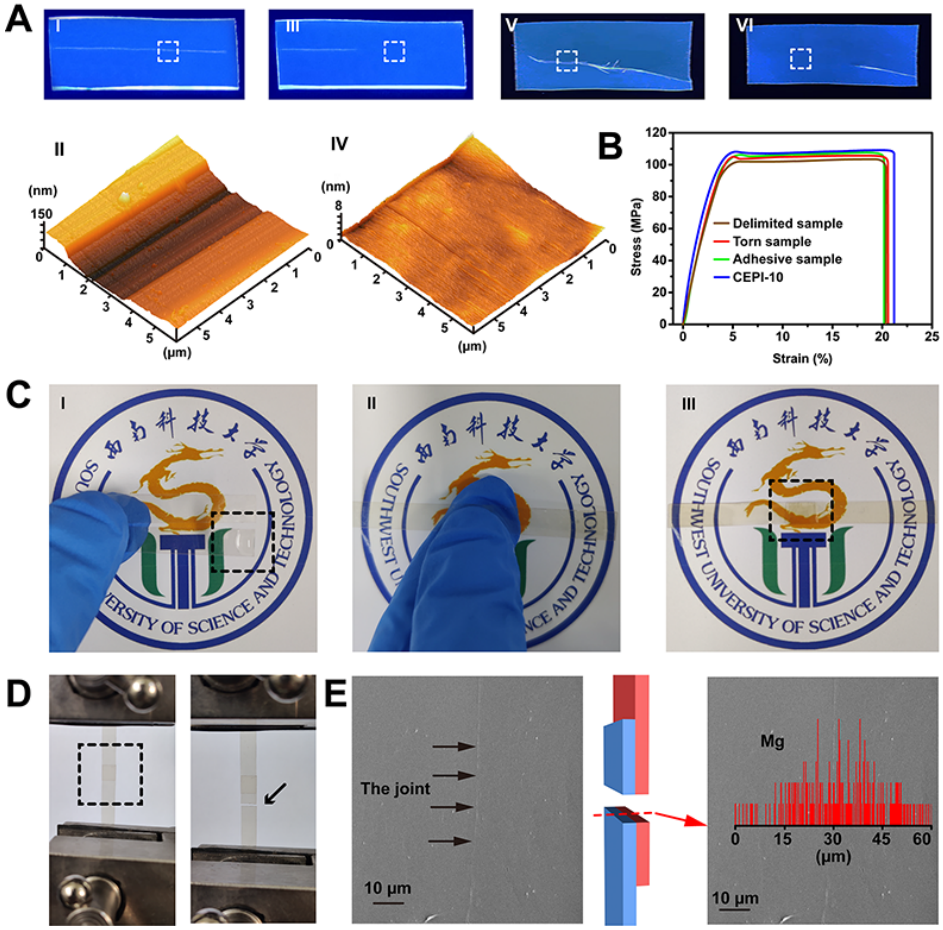

Figure 5. A photograph of CEPI-10 film showing a well-defined cut (I in A), and healing after Mg-ion solution treatment under UV light (III in A). Atomic force microscope (AFM) images of a damaged CEPI-10 film before healing (II in A) and after healing (IV in A). A torn CEPI-10 film (V in A) and healing after Mg-ion solution treatment under UV light (VI in A). (B) The mechanical properties of the different films. The contact region is pretreated with a small drop of NMP (I in C). Bringing two pieces into contact by slight pressing (II in C), and the two films are adhered together (III in C). (D) Sample to stretch and the broken sample after stretching. (E) SEM image and the EDX Mg line scan along the cross section.

The dynamic nature of supramolecular crosslinking within the thermosets also enable the adhesion between two solid pieces of thermosets. Mg-ion solution is added between the surface of the two pieces of CEPI-10 films, followed by a slight pressing for 1 min to establish the interfacial indole-Mg-indole interaction at the interface (I, II in Figure 5C). The adhered area of approximately 1 cm^2 (III in Figure 5C). Stress-strain experimentation is performed for the adhered sample, and it has nearly the same stress-strain behaviors with the original CEPI-10 sample (Figure 5B). Moreover, It is found that the integrated thermoset breaks but not at the adhered area (Figure 5D), suggesting a strong adhesion between the two thermosets.[16] SEM image shows that the polymer chains diffuse naturally into each other parts crossing the adhered area, and the two surfaces are fully integrated (I in Figure 5E). In addition, energy dispersive x-ray spectroscopy (EDX) Mg line scan (red curve) along the cross section of the sample is used to verify the adhesive mechanism. Mg shows a normal distribution along the cross section (II in Figure 5E), indicating that indole-Mg-indole interaction is reestablished crossing the adhered area.

3. Conclusions

The indole-Mg-indole supramolecular approach for high-performance thermosets described herein enables a combination of exceptional mechanical properties as well as a range of stimuli-responsive functions for healing, recycling and adhesion. Our approach differs significantly from traditional supramolecular approaches, such as dynamic hydrogen bonding, electrostatic and metal-ligand interactions, to produce thermosets. In this approach, the breaking of indole-

Mg-indole bond requires an extraordinary external force (comparable to that for breaking the C-C covalent bonding) and the indole-Mg-indole bond recovers immediately due to the supramolecular nature of the bonding. This allows an effective energy dissipation when an external force is applied. The key innovation of our approach is thus the use of the noncovalent sandwich-structural indole-Mg-indole complexes acting as the energetic crosslinking points for construction of force-activatable crosslinks that can be installed in the solid state without any external stimulus. Such ambient force-activated reversible indole-Mg-indole crosslinking could thus be potentially considered as a general method for the design of toughened and multifunctional high-performance thermosets.

4. Experimental Section

Materials: Epoxide resin (e51, Macklin, cas: 61788-97-4). EPI synthesis: e51 (1.96 g, 10 mmol, 1 eq), tryptamine (1.6 g, 10 mmol, 1 eq) were dissolved in DMF (5 mL) and reacted at 80 °C for 12 h, M_n = 51100, M_w = 114200, M_w/M_n = 2.23. All other chemicals and solvents were analytical reagents and used as received without further purification.

Faberation of the CEPI-10 film: To a solution of linear EPI was slowly added a certain amount of $Mg(Ot\text{-}Bu)_2$ solution in N, N-dimethylformamide (DMF) (mole ratio of $Mg(Ot\text{-}Bu)_2$: indole = 1 : 10). 2.0 g EPI, 96 mg $Mg(Ot\text{-}Bu)_2$, 15mL DMF. The mixed solution was filtered and casted on a clean glass sheet (75 mm * 25 mm), dried at 80 °C for 8 h under vacuum. After cooling to room temperature slowly, the film with glass slide was soak in distilled water for 3 hours and the film can be easily peeled off from the glass slide. Under vacuum condition, the wet film was dried at 30 °C for 24 h to remove water molecules from the film.

Supporting Information

Supporting Information is available from the Wiley Online Library or from the author.

Acknowledgements

This work was supported by the National Natural Science Foundation of China (21973076 and 22006122), the Sichuan Talent Fund for Distinguished Young Scholars (2021JDJQ0033), the Applied Basic Research Programs of Sichuan Science and Technology Department (2021YJ0059), the Innovation and Development Fund of China Academy of Engineering Physics (CX20210039). Guanjun Chang and Li Yang are grateful for financial support from the China Scholarship Council. We thank the Southwest Computing Center of the China Academy of Physics Engineering for their support of computer simulation.

Received: ((will be filled in by the editorial staff))
Revised: ((will be filled in by the editorial staff))
Published online: ((will be filled in by the editorial staff))

References

[1] a) E. Filippidi, T. R. Cristiani, C. D. Eisenbach, J. H. Waite, J. N. Israelachvili, B. K. Ahn, M. T. Valentine, *Science* **2017**, *358*, 502; b) G. Chang, L. Yang, J. Yang, M. P. Stoykovich, X. Deng, J. Cui, D. Wang, *Adv. Mater.* **2018**, *30*, 1704234; c) H. J. Meredith, J. J. Wilker, *Adv. Funct. Mater.* **2015**, *25*, 5057.

[2] a) M. Sharif, G. R. Palmese, *J. Mater. Chem. A* **2021**, *9*, 1014; b) B. J. Rohde, K. M. Le, R. Krishnamoorti, M. L. Robertson, *Macromolecules* **2016**, *49*, 8960.

[3] a) D. S. Kim, K. Cho, J. K. Kim, C. E. Park, *Polym. Eng. Sci.* **1996**, *36*, 755; b) J. S. Bergstrom, M. C. Boyce, *Rubber Chem. Technol.* **1999**, *72*, 633; c) N. Sheng, M. C. Boyce, D. M. Parks, G. C. Rutledge, J. I. Abes, R. E. Cohen, *Polymer* **2004**, *45*, 487.

[4] a) R. J. Wojtecki, M. A. Meador, S, J. Rowan, Nat. Mater. 2011, 10, 14; b) T. L. Sun, T. Kurokawa, S. Kuroda, A. B. Ihsan, T. Akasaki, K. Sato, M. A Haque, T. Nakajima, J. P. Gong, *Nat. Mater.* **2013**, *12*, 932; c) J. Liu, C. S. Y. Tan, Z. Yu, Y. Lan, C. Abell, O. A. Scherman, *Adv. Mater.* **2017**, *29*, 1604951; d) Y. Zhuo, Z. Xia, Y. Qi, T. Sumigawa, J. Wu, P. Šesták, Y. Lu, V. Håkonsen, T. Li, F. Wang, W. Chen, S. Xiao, R. Long, T. Kitamura, L. Li, J. He, Z. Zhang, *Adv. Mater.* **2021**, *33*, 2008523; e) X. Lu, C. Bao, P. Xie, Z. Guo, J. Sun, *Adv. Funct. Mater.* **2021**, *31*, 2103061.

[5] a) J. Meurer, J. Hniopek, T. Bätz, S. Zechel, M. Enke, J. Vitz, M. Schmitt, J. Popp, M. D. Hager, U. S. Schubert, *Adv. Mater.* **2021**, *33*, 2006655; b) J. A. Neal, N. J. Oldenhuis, A. L. Novitsky, E. M. Samson, W. J. Thrift, R. Ragan, Z. Guan, *Angew. Chem. Int. Ed.* **2017**, *56*, 15575; c) S. Li, N. Chen, X. Li, Y. Li, Z. Xie, Z. Ma, J. Zhao, X Hou, X. Yuan, *Adv. Funct. Mater.* **2020**, *30*, 2000130.

[6] a) E. Ducrot, Y. Chen, M. Bulters, R. P. Sijbesma, C. Creton, *Science* **2014**, *344*, 186; b) P. Lechtken, *Chem. Ber.* **1976**, *109*, 2862; c) H. Zhang, X. Li, Y. Lin, F. Gao, Z. Tang, P. Su, W. Zhang, Y. Xu, W. Weng, R. Boulatov, *Nat. Comm.* **2017**, *8*, 1147.

[7] a) Y. Tian, X. Cao, X. Li, H. Zhang, C. Sun, Y. Xu, W. Weng, W. Zhang, R. Boulatov, *J. Am. Chem. Soc.* **2020**, *142*, 18687; b) J. Wang, T. B. Kouznetsova, R. Boulatov, S. L. Craig, *Nat. Comm.* **2016**, *7*, 13433; c) Y. Tian, R. Boulatov, *ChemPhysChem* **2012**, *13*, 2277.

[8] a) J. C. Ma, D. A. Dougherty, *Chem. Rev.* **1997**, *97*, 1303; b) S. Yamada, *Chem. Rev.* **2018**, *118*, 11353; c) T. Sheikh, S. Maqbool, P. Mandal, A. Nag, *Angew.Chem. Int.Ed.* **2021**, *60*, 18265.

[9] a) H. Yorita, K. Otomo, H. Hiramatsu, A. Toyama, T. Miura, H. Takeuchi, *J. Am. Chem. Soc.* **2008**, *130*, 15266. b) X. Guan, Y. Ma, L. Yang, Y. Xu, Y. Lan, Y. Huang, T. P. Diangha, G. Chang, *Chem. Commun.* **2020**, *56*, 1054.

[10] a) L. J. Juszczak, A. S. Eisenberg, *J. Am. Chem. Soc.* **2017**, *139*, 8302; b) Y. Li, M. Du, L. Yang, Y. Bao, Y. Xu, Q. Yin, Y. Lan, G. Chang, *Chem. Eng. J.* **2021**, *414*, 128820.

[11] a) S. Akbulatov, Y. Tian, R. Boulatov, *J. Am. Chem. Soc.* **2012**, *134*, 7620; b) T. J. Kucharski, R. Boulatov, *J. Mater. Chem.* **2011**, *21*, 8237.

[12] a) S. Timoshenko, J. N. Goodier, *Theory of Elasticity*, International Editions, McGraw Hill, USA **1970**; b) I. M. Ward, J. Sweeney, *Introduction to the Mechanical Properties of Solid Polymers*, John Wiley & Sons Ltd, USA **2004**; c) A. R. Tripathy, J. E. Morin, D. E. Williams,

S. J. Eyles, R. J. Farris, *Macromolecules* **2020**, *35*, 4616; d) S. Uemura, Y. Matsuo, T. Okamatsu, T. Arita, M. Shimomura, Y. Hirai, *Adv. Eng. Mater.* **2020**, *22*, 1901226.

[13] a) I. M. Ward, *Mechanical Properties of Solid Polymers*, John Wiley & Sons, New York **1983**, Ch. 2; b) L. H. Sperling, *Introduction to Physical Polymer Science*, John Wiley & Sons, New York **2006**, Ch.11; c) D. I. Bower, *An Introduction to Polymer Physics*, Cambridge University Press, Cambridge, UK **2002**, Ch. 6, 8.

[14] a) M. Du, L. Yang, C. Liao, T. P. Diangha, Y. Ma, L. Zhang, Y. Lan, G Chang, *Macromol. Rapid Commun.* **2020**, *41*, 1900606; b) L. Cao, L. Yang, Y. Xu, Q. Yin, Y. Huang, G. Chang, *Macromol. Rapid Commun.* **2021**, *42*, 2000617; c) P. Dastidar, S. Ganguly, K. Sarkar, *Chem. Asian J.* **2016**, *11*, 2484.

[15] a) A. Pena-Francesch, H. Jung, M. C. Demirel, M. Sitti, *Nat. Mater.* **2020**, *19*, 1230; b) M. Khatib, O. Zohar, W. Saliba, H. Haick, *Adv. Mater.* **2020**, 32, 2000246; b) S. Li, L. Wang, W. Zheng, G. Yang, X. Jiang, *Adv. Funct. Mater.* **2020**, *30*, 2002370; c) J. Zhu, Y. Cheng, S. Hao, Z. L. Wang, N. Wang, X. Cao, *Adv. Funct. Mater. 2021, 31*, 2100039.

[16] a) G. Chang, L. Yang, J. Yang, M. P. Stoykovich, X. Deng, J. Cui, D. Wang, *Adv. Mater.* **2018**, *30*, 1704234; b) Y. Gao, J. Chen, X. Han, Y. Pan, P. Wang, T. Wang, T. Lu, *Adv. Funct. Mater.* **2020**, *30*, 2003207; c) C. Cui, W. Liu, *Prog. Polym. Sci.* **2021**, *116*, 101388.

Force-reversible high-performance thermosets are prepared using indole-Mg-indole interaction as crosslinking. The energetic indole-Mg-indole interaction can be reversibly installed and removed by force perturbation at at ambient conditions, making these thermosets with excellent mechanical properties and multiple stimuli-responsive functions, such as recyclability; healability and adhesion.

Li Yang, Yicheng Li, Mengqi Du, Yiting He, Yang Lan,* Qiang Yin, Fanghua Zhu and Guanjun Chang*

Force-Reversible and Energetic Indole-Mg-Indole Interaction for Designing Toughened and Multifunctional High-Performance Thermosets

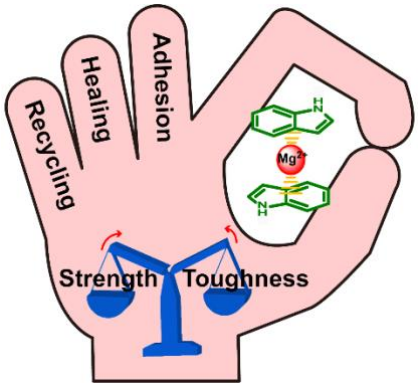

Supporting Information

Force-Reversible and Energetic Indole-Mg-Indole Interaction for Designing Toughened and Multifunctional High-Performance Thermosets

Li Yang, Yicheng Li, Mengqi Du, Yiting He, Yang Lan, Qiang Yin, Fanghua Zhu and Guanjun Chang**

Methods

^{1}H Nuclear Magnetic Resonance (^{1}H NMR)

^{1}H NMR spectra were recorded on a Bruker AMX600 MHz NMR spectrometer within DMSO-d_6, depending on the solubility of the material in these solvents. The chemical shift are represented in δ (ppm) with $SiMe_4$ as internal standard at room temperature.

Fourier Transform Infrared Spectroscopy (FTIR)

FTIR spectra were measured as KBr pellets on a Nicolet 6700 FTIR spectrometer equipped with a deuterated triglycine sulfate (DTGS) detector and a Ge/KBr beam splitter. Or treated quartz sheets by casting the polymer were placed in sample pool to measure polymer structure. Data collection was performed by Thermo Nicolet, version 7.0, in an OMNIC operating system that connects to the spectrometer. FTIR spectra were recorded from 32 scans at a resolution of 4 cm^{-1} in the range of 4000-400 cm^{-1}. The final spectra were subtracted by an air spectrum to remove the background.

Scanning electron microscopy (SEM) and energy dispersive X-ray spectroscopy (EDX)

Ground particles of CPMMA were sputter coated with gold/palladium 60/40, 99.99% (Cressington 208HR) for 60 seconds. SEM images were obtained on a field emission scanning electron microscope (Zeiss Ultra 55, Germany) with EDX operating at a 10 kV accelerating voltage.

Ultraviolet/visible Light (UV/vis) Absorption Spectroscopy

UV/vis absorption spectra were measured as absorption mode using UV-2600, which was equipped with integrating sphere when testing polymer films. Solid UV/vis absorption spectra were measured by placing a polymer coated quartz sheet in the passageway of incident light

using quartz sheet as the background. Both of stretching sample and simple the fixture device were directly placed in the passageway of incident light to test the relaxation–UV/vis absorption spectra in situ. About 20 um thick films were prepared by spin coating method. Converting transmission-wavenumber to adsorption-wavenumber is according to the Beer-Lambert law.

Fluorescence Emission Spectrum

The fluorescence emission spectrum including in situ relaxation–RF spectrum, were performed by using a RF-6000 spectrophotometer. The emission spectra (400-700 nm) were recorded using an excitation wavelength of 365 nm and 5 nm (excitation)/5 nm (emission) slit widths. The stretching sample and the simple fixture device was directly placed in sample pool to test the in situ relaxation–RF spectrum.

Tensile Testing

Uniaxial tensile testing was carried out on electromechanical universal tester machine (MTS, CMT4304) with 50N sensor at a strain rate of 2 mm/min and a temperature of 25 °C. The dimension of the casting film samples: 50.00 mm × 10.00 mm × 0.12 mm; The dimension of the remodeling sample was showed in Scheme S1. The stress at break and elongation at break were obtained from the stress-strain experiment with at least three identical specimens and reported as averaged values.

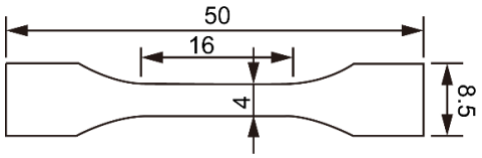

Scheme S1. The dimension (mm) of the remodeling sample

Stress Relaxation

The stress relaxation experiments were carried out on electromechanical universal tester machine (MTS, CMT4304). Samples were first loaded uniaxially at a strain rate of 2 mm/min to a strain of 10 %. Load and strain are measured with time at constant grip displacement.

Quantum-Chemical Calculations

All computation was carried out with the Gaussian 16 Revision A.03 software package. The Berny algorithm was used to locate stationary points. Different conformations are set through

increasing the distance between ion and indole plane. Very tight convergence criteria and ultrafine integration grids were used in all optimizations. The calculations of analytical frequencies on converged constrained molecules are valid because the molecule plus its infinitely-compliant constraining potential is a stationary point.[1,2] To start with, the B3LYP/6-31+G(d,p) level of theory[3] was used for geometry optimizations. The B3LYP functional has been proven to produce good geometries but is less accurate for energy calculations. Therefore energies were refined with the M06-2X functional,[4,5] which is able to account for dispersion effects, and a 6-31++G(d,p) basis set. Viewing atomic forces is through GaussView, and the binding energy is the inverse of the area as a function of force and distance.

Characterization of EPI and CEPI-10

The detailed procedure for the synthesis of EPI and CEPI were given in *Experimental Section*. The fourier transform infrared spectroscopy (FTIR) and ^{1}H nuclear magnetic resonance (^{1}H NMR) of EPI and CEPI are showed in Figure S1 and Figure S2. *EPI*: 13C CP/MAS NMR, δ: 154, 141, 135, 125, 117, 111, 68, 55, 39, 29. IR (KBr) ν: 740, 822, 1579, 1609, 1661, 2921, 3432 cm^{-1}. *CEPI-10*: 13C CP/MAS NMR, δ: 154, 141, 135, 127, 117, 112, 68, 55, 39, 29. IR (KBr) ν: 741, 824, 1575, 1609, 1663, 2925, 3429 cm^{-1}.

In Figure S1, The characteristic peaks of both EPI and CEPI-10 films does not exhibit any shifts with each other. Compared with EPI, We found that the intensity of C=C skeleton stretching vibration peak at 1609 cm^{-1} in CEPI-10 decreased significantly, likely reflecting a change in the extinction coefficient of the indole group when indole-Mg-indole interaction formation.[6,7]

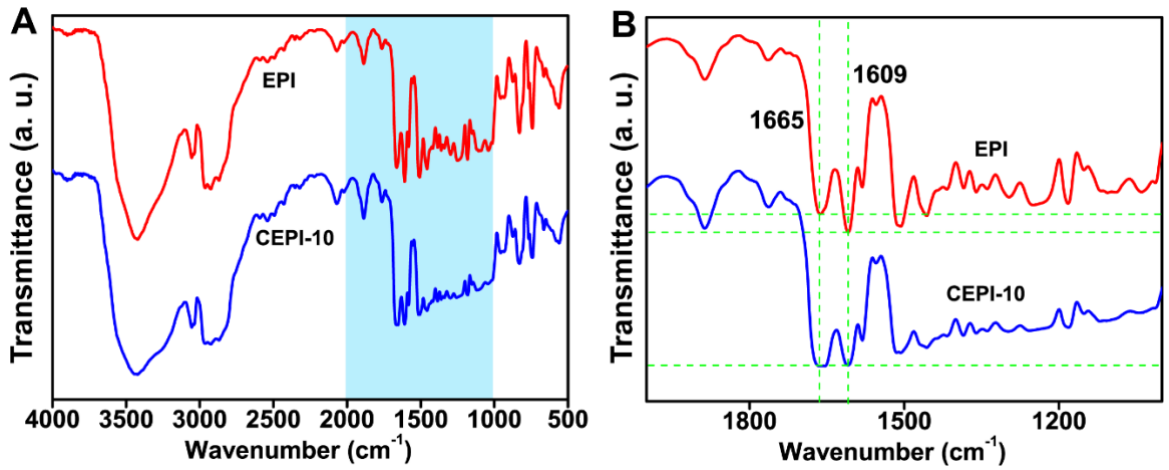

Figure S1. FTIR spectrum of as-synthesized EPI and CEPI-10.

The structural information of the prepared EPI and CEPI-10 was also obtained by ^{13}C CP/MAS NMR (Figure S2). There are broad signals at 100–150 ppm ascribed to aromatic group carbons. The signal shifted at range of 100-150 ppm of CEPI-10 are induced by indole-Mg-indole interaction formation.[7]

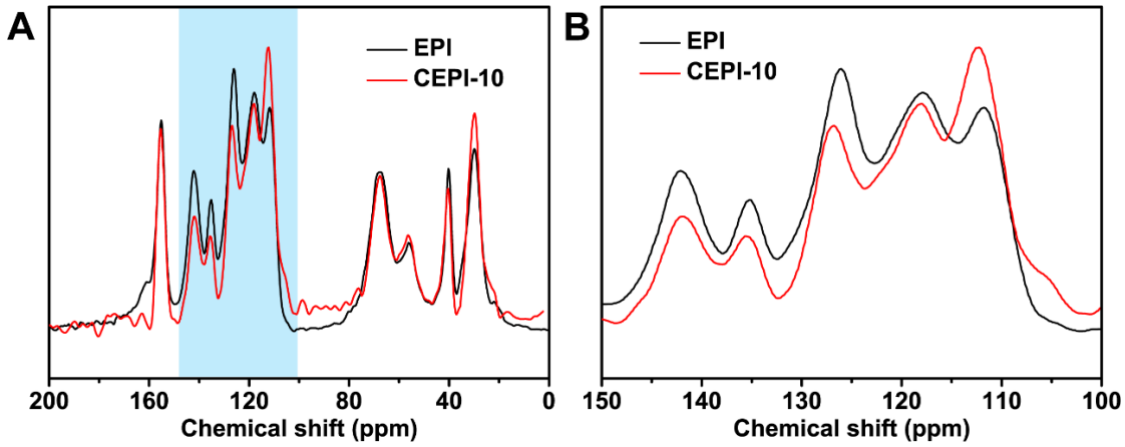

Figure S2. ^{13}C CP/MAS NMR spectrum of as-synthesized EPI and CEPI-10.

Physical properties of the EPI and CEPI films

The thin film of CEPI-10 film is readily prepared by the solution casting technique using NMP as a solvent. And the CEPI-10 film (thickness: ca. 120 μm) exhibited excellent optical transparency (Figure S3). EPI possess good solubility in common organic solvents, such as

NMP, DMF, DMAc, and DMSO. The crosslinked CEPI films can not disolved in any solvents, which indicate the formation of cross-linked networks.

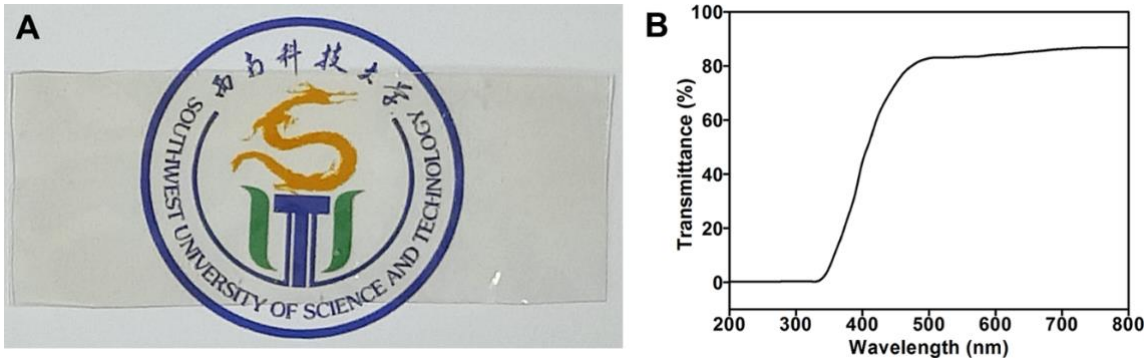

Figure S3. (A) The photo of the CEPI-10 film; (B) UV–vis spectrum of the CEPI-10 film.

Table S1. Solubility of the polymer films in different solvents

Sample	DMAc[a]	DMSO[b]	DMF[c]	NMP[d]	THF[e]
EPI	+[e]	+	+	+	-
CEPI-5	-	-	-	-	-
CEPI-10	-	-	-	-	-
CEPI-15	-	-	-	-	-
CEPI-20	-	-	-	-	-

[a]*N*,*N*-Dimethylacetamide (DMAc); [b]Dimethyl Sulfoxide (DMSO); [c]*N*,*N*-Dimethylformamide (DMF); [d]*N*-Methyl-2-pyrrolidone (NMP); [e]Tetrahydrofuran (THF); +: The polymer can be completely dissolved at room temperature; -: the polymer was insoluble at room temperature.

Thermo properties of EPI and CEPI-10 films

The use of advanced polymers in many practical application depends on their environmental and thermal stabilities.[8] In this work, thermal properties of EPI and CEPI-10 films were evaluated via TGA (Figure S4A). TGA curves suggest that the polymers are thermally stable up to 350 ^{o}C. Compared with EPI, the CEPI-10 film shows a higher decomposition temperature (~368 ^{o}C) owing to the construction of the crosslinking networks.

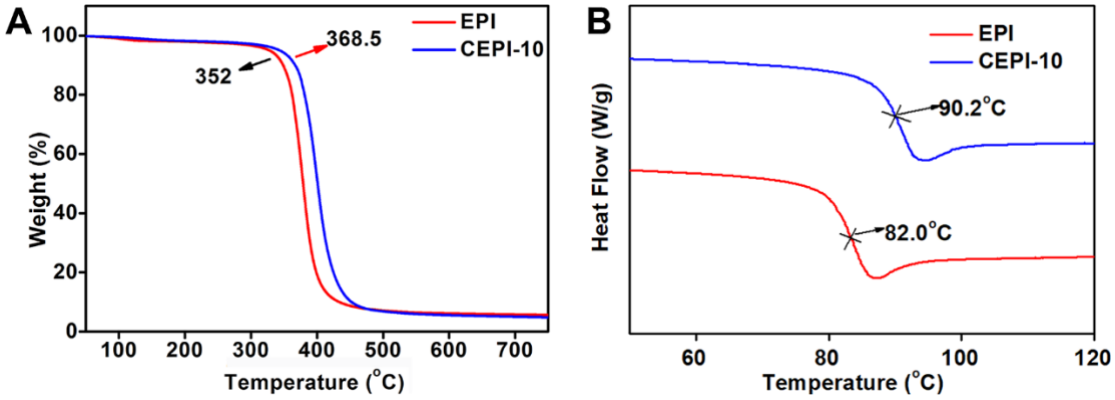

Figure S4. Spectrum of as-synthesized EPI and CEPI-10.

Differential scanning calorimetry (DSC) of CEPI-10 film up to ~ 90 ºC shows a single Tg, The DSC thermograms of the polymers are shown in Figure S4B. Due to the crosslinking networks in CEPI-10, the Tg of CEPI-10 film is higher than that of the linear EPI.

SEM image of the cross section for the broken sample after stretching

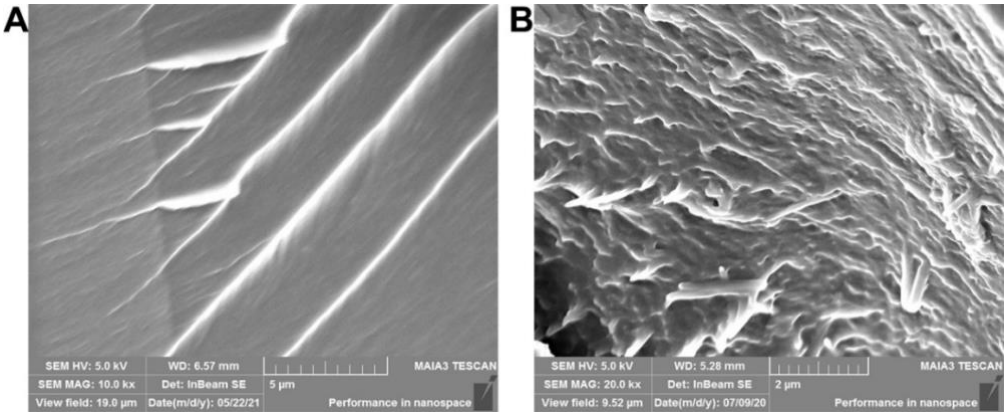

Figure S5. Spectrum of as-synthesized EPI and CEPI-10.

Mechanical properties of different themosets

To further understand the mechanical properties of the CEPI-10 themoset, here we compared the mechanical properties between CEPI-10 and related traditional thermosets (Figure S6A). We chose $Zn(CH_3COO)_2$, $Mn(CH_3COO)_2$, $Ni(CH_3COO)_2$, $Cu(CH_3COO)_2$,

$Mg(CH_3COO)_2$, $Ba(Ot\text{-}Bu)_2$ and $Mg(Ot\text{-}Bu)_2$ as the crosslinking sites of the polymers. The mechanical properties of the different polymer films is shown in Figure S6B.

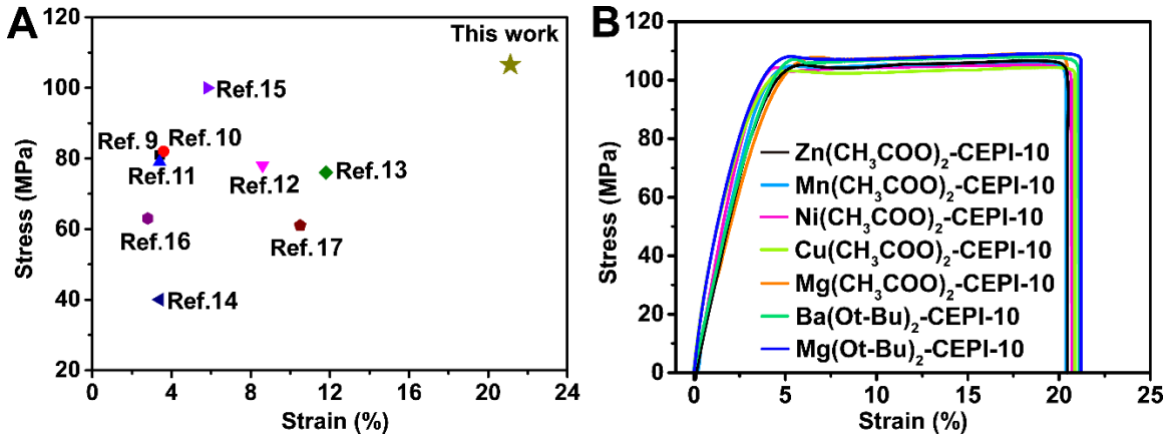

Figure S6. Stress-strain curves of different polymer films.

References

1 T. J. Kucharski, R. Boulatov, *J. Mater. Chem.* **2011**, *21*, 8237.

2 G. S. Kochhar, G. S. Heverly-Coulson, N. J. Mosey, in *Polymer Mechanochemistry* (ed Roman Boulatov) 37–96 (Springer International Publishing, **2015**).

3 C. T. Lee, W. T. Yang, R. G. Parr, *Phys. Rev. B* **1988**, *37*, 785.

4 Y. Zhao, D. G. Truhlar, *Theor. Chem. Acc.* **2008**, *120*, 215.

5 L. Liu, D. Malhotra, R. S. Paton, K. N. Houk, G. B. Hammond, *Angew. Chem., Int. Ed.* **2010**, *49*, 9132.

6 R. Wang, T. Xie, *Chem. Commun.* **2010**, *46*, 1341.

7 G. Chang, L. Yang, J. Yang, M. P. Stoykovich, X. Deng, J. Cui, D. Wang, *Adv. Mater.* **2018**, *30*, 1704234.

8 a) D. Shukla, Y. Negi, J. Uppadhyaya, V. Kumar, *Polym. Rev.* **2012**, *52*, 189; b) D. Liaw, K. Wang, Y. Huang, K. Lee, J. Lai, C. Ha, *Prog. Polym. Sci.* **2012**, *37*, 907.

9 T. Wu, Y. Liu, N. Li, G.-W. Huang, C.-B. Qu, H.-M. Xiao, *Polym. Test.*, **2019**, *74*, 45.

10 H. Duan, Y. Chen, S. Ji, R. Hu, H. Ma, *Chem. Eng. J.*, **2019**, *375*, 121916.

11 Y. Tian, Q. Wang, L. Shen, Z. Cui, L. Kou, J. Cheng, J. Zhang, *Chem. Eng. J.*, **2020**, *383*, 123124.

12 X.-F. Liu, B.-W. Liu, X. Luo, D.-M. Guo, H.-Y. Zhong, L. Chen, Y.-Z. Wang, *Chem. Eng. J.*, **2020**, *380*, 122471.

13 S. Li, H. Wang, M. Liu, C. Peng, Z. Wu, *J. Appl. Polym. Sci.*, **2019**, *136*, 46930.

14 X.-G. Li, M.-R. Huang, L.-H. Zhu, Y. Yang, *J. Appl. Polym. Sci.*, **2001**, *82*, 790.

15 B.J. Rohde, K.M. Le, R. Krishnamoorti, M.L. Robertson, *Macromolecules*, **2016**, *49*, 8960.

16 Y. Qi, J. Wang, Y. Kou, H. Pang, S. Zhang, N. Li, C. Liu, Z. Weng, X. Jian, *Nat. Commun.*, **2019**, *10*, 2107.

17 L. Xiao, J. Huang, Y. Wang, J. Chen, Z. Liu, X. Nie, *ACS Sustain. Chem. Eng.*, **2019**, *7*, 17344.